Comparison of different image processing techniques for VIS-NIR images in maritime environments at night

Tristan Preis
Institute for the Protection of Maritime Infrastructures
German Aerospace Center (DLR e.V.)
Bremerhaven, Germany
Tristan.Preis@dlr.de

Laura Kontschak
Institute for the Protection of Maritime Infrastructures
German Aerospace Center (DLR e.V.)
Bremerhaven, Germany
Laura.Kontschak@dlr.de

Alexander Klein
Institute for the Protection of Maritime Infrastructures
German Aerospace Center (DLR e.V.)
Bremerhaven, Germany
Alexander.Klein@dlr.de

Jendrik Schmidt
Institute for the Protection of Maritime Infrastructures
German Aerospace Center (DLR e.V.)
Bremerhaven, Germany
Jendrik.Schmidt@dlr.de

Maurice Stephan
Institute for the Protection of Maritime Infrastructures
German Aerospace Center (DLR e.V.)
Bremerhaven, Germany
Maurice.Stephan@dlr.de

Enno Peters
Institute for the Protection of Maritime Infrastructures
German Aerospace Center (DLR e.V.)
Bremerhaven, Germany
Enno.Peters@dlr.de

***Abstract*—In the maritime environment, visual (VIS) and infrared (IR) imaging systems are used for various applications, including navigation, situational awareness, and search and rescue operations. These scenarios share the need for object detection, especially in harsh environments at night and bad weather conditions. This study presents a comprehensive comparison of post-processing techniques, such as sensor specific noise reduction by a non-uniformity correction (NUC), stochastic (random) noise reduction, with Gaussian and fast Fourier transform (FFT) filtering, and contrast enhancement, with three tone mapping operators (Reinhard, Mantiuk and Drago).**

The experimental evaluation comprises analysis of image quality metrics such as signal-to-noise ratio (SNR) and contrast evaluation. As a result, a decision must be made as to whether reduce the noise or increase the contrast, as the combinations of the methods presented cannot realize both improvements at the same time. Overall, image post-processing can improve the detection of objects at sea and night for a human operator.

***Index Terms*—image processing, visibility improvement, visible and infrared imaging, maritime environment, search and rescue operations (SAR)**

I. INTRODUCTION

Optical systems in both, visible to near infrared (in the following denoted as VIS-NIR) and thermal infrared (in the following denoted as IR), are widely used on ships for various tasks, including navigation at night or search and rescue missions. In particular, these systems are used by rescue operators and law enforcement agencies. The intention is, that the operator can search for objects or persons in the water from a protected location. This is particularly helpful in situations with rough seas and poor weather conditions, such as rain and strong winds. In contrast to IR, which uses thermal radiation emitted by the environment itself, using VIS-NIR system at night is more challenging, as there is little light available and therefore usually requiring active illumination. By using large receiving optics, the amount of light collected can be increased, but this method reaches its limits due to the increasing size and costs of the camera system. Another option is to process the image with post-processing methods so that the objects of interest stand out more from the visible image. Obviously this approach is limited as well, ultimately by photon shot noise (Poisson noise), but can nevertheless improve the image quality to some extent and thus helping the identification and detection of objects at night.

This study focuses more on basic post-processing methods to enhance the image quality (and correspondingly the visibility) of VIS-NIR images, than was the case in Preis et al. [1]. In that paper, first a non-uniformity correction (NUC) and then a contrast enhancement algorithm was performed, using an equivalent system like in this study. It was the first attempt to post-process VIS-NIR images beyond a NUC. The equalizer used, delivered good results, but had not yet been used in literature. For this reason, basic image processing methods, discussed in literature, are used in this study. These should then form a basis for further processing methods in the future.

Nevertheless, Preis et al. [1] serves as a starting point,

as it was found that a 1-point NUC is sufficient to reduce the sensor-specific noise in mainly dark images. Then, in the second step, the stochastic noise is reduced, using two basic filter methods. These are the Gaussian filter and the fast Fourier transform (FFT). In the third step, one of the three tone mapping operators according to Reinhard [2], Mantiuk [3] and Drago [4] is applied to the filtered images. The operators differ from each other in the extent, to which they increase the contrast for the human eye through non-linear adjustments. These algorithms serve the same purpose as the equalizer from Preis et al. [1].

Tone mapping is especially promising, when the instrument provides raw image formats with pixel depths larger than 8 bit, which need to be scaled down to 8 bit for displays anyway. Besides the presented tone mapping operators, there are also other methods to increase the contrast in monochrome images like in Yelmanov and Romanyshyn [5].

It is also investigated, whether these image improvements can be qualitatively determined by a signal-to-noise ratio (SNR) and contrast evaluations according to the Michelson contrast (C_M) [6] and contrast-to-noise ratio (CNR). This paper therefore deals with the post-processing of images in the VIS-NIR range taken with a high sensitivity monochrome 12-bit camera at night. For comparison purposes, an IR camera was also used.

II. INSTRUMENTS, SETUP AND FIELD CAMPAIGN

During a three-day trip in the German Bight with the Federal Maritime and Hydrographic Agency (Bundesamt für Seeschifffahrt und Hydrographie, BSH) in March 2024, a data set consisting of nighttime images was collected. An in-house developed multi-sensor head, that was mounted on a PTU, was used. The multi-sensor system comprised a VIS-NIR camera, a laser illuminator emitting light at 808 nm, for actively illuminating a scenery, and a IR camera. The VIS-NIR camera and laser illuminator was developed as a system with a field of view (FOV) of 7° x 6° in the project TRAGVIS [7] to obtain a low-cost range-gated viewing system.

In this study range-gated viewing is used to record a scene, while reducing backscattering by excluding specific regions depending on the distance from the system. Consequently, the resulting image has information of a specified area with a defined width and distance only, called 'gate'. In these measurements, the first 50 m of a scene were not recorded, as these have the highest proportion of backscatter.

In addition to the range-gated system the multi-sensor instrument contains the IR camera PI 640i from Optris. It has a resolution of 640 x 480 pixels and has a FOV of 15° x 12°. Because of the larger field of view and the fact that the environment itself emits thermal radiation, i.e. the world is bright in a thermal image, during the routine operation of the system, the IR camera was used to get an overview, and the VIS-NIR system with active illumination was used for a more detailed inspection of objects of interests or unclear objects showing up in the IR images.

The multi-sensor system was mounted at the pan-tilt-unit (PTU) PTU-D300E from FLIR, enabling to adjust direction and inclination of the system. At high waves, the integrated sea state stabilization was used as well. The housing of all components were designed to withstand the harsh environment of the North Sea. Figure 1 shows the setup on the traverse of the BSH ship ATAIR.

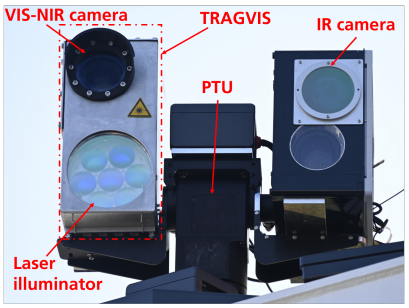

Fig. 1. Range-gated viewing system (VIS-NIR camera and laser illuminator) installed on a pan-tilt-unit (PTU) including an IR-camera (black box) on the traverse of the BSH ship ATAIR

The field campaign was held at night times from March 09-12, 2024 in the German Bight as part of other campaigns of the BSH on board of the ATAIR. The visibility was 7 km and thus excluding backscattering from the first 50 m in range-gating mode turned out to be sufficient to eliminate all visible atmospheric backscattering in the images.

III. IMAGE POST-PROCESSING ALGORITHMS

In the first step, sensor specific noise is reduced, caused by non-uniform behaviour in terms of dark signal and response of the different pixels across the image sensor (Sec. III-A). Afterwards stochastic (random) noise is decreased from each image, by filtering specific frequencies of the image (Sec. III-B). These steps are crucial, because tone mapping algorithms used later (Sec. III-C), can enlarge the noise in specific regions of an image.

A. NON-UNIFORMITY CORRECTION

The first and most simple algorithm to reduce noise is a 1-point NUC [8]. First, a dark image $\boldsymbol{x}_{ref,dark}$ is acquired with the shutter closed. To reduce temporal noise, the dark image consists of 100 individual images that have been averaged. When subtracted from a measured image $\boldsymbol{x}_0$

$$\boldsymbol{x}_{1-NUC} = \boldsymbol{x}_0 - \boldsymbol{x}_{ref,dark} \tag{1}$$

the so-called dark signal non-uniformity (DSNU), i.e. systematic structures in the dark signal, can be compensated. The resulting image is subsequently dark. This can be problematic as the human eye can perceive differences between bright gray levels better than between dark gray levels [9]. Therefore, the average of the dark reference image $\overline{x_{ref,dark}}$ can be added to the resulting image, leading to the same average gray value of the original image

$$\boldsymbol{x}_{1-NUC,mean} = \boldsymbol{x}_{obj} - \boldsymbol{x}_{ref,dark} + \overline{x_{ref,dark}} \tag{2}$$

DOI: 10.5281/zenodo.17119990

Normally, a 2-point NUC is used to reduce the noise caused from Photo Response Non-Uniformity (PRNU), but for mainly dark images acquired in gated mode as it is typical, when observing small objects at sea during darkness, this algorithm offers no benefit in contrast to the 1-point NUC [1].

B. STOCHASTIC NOISE REDUCTION

After the non-uniformity correction stochastic noise is still present. To reduce this type of noise, a filter can be applied that suppresses certain spatial frequencies. [10].

A simple low-pass is a Gaussian filter [11], in which the resulting gray value of a pixel is calculated depending from its surrounding pixels. This leads to a standardization in a certain radius around the pixel. In practice, a 2D mask with a Gaussian distribution is applied to the image and calculated individually for each pixel. The larger the mask and the Gaussian distribution, the less strongly edges are displayed in the image. The width of the Gaussian distribution should be therefore carefully chosen, to reduce random noise, like single pixels, that are brighter or darker, than their surrounding, and, at the same time, not reduce structures like the hull of a ship. For this reason the $OpenCV$ [12] function $GaussianBlur$ [13] was used. The function is designed to blur, respectively low-pass filter, an image depending on the kernel size (2D mask) of the function.

Alternatively, to suppress certain noisy frequencies in the image, a FFT can also be performed. In the course of this study, the Python module $fftpack$ [14] was used, to convert the image into the frequency domain. In the frequency domain, noise can be reduced depending on the frequency by masking. Therefore, a mask with 1s and 0s of the same size as the transformed image is multiplied. The parts of the frequency multiplied with 1 are present after transforming back to the image domain, the parts multiplied with 0 are neglected.

C. TONE MAPPING

The last step investigated, for enhancing an image used in the context of this study, are global tone mapping operators proposed by Reinhard [2], Mantiuk [3] and Drago [4], which are individually applied. These are three classic methods and build a starting point for displaying a high dynamic range (HDR) image optimized for a display with a lower bit depth. The resulting image should have better perceptibility of objects for the human eye, displayed on a screen or printed image.

Reinhard's algorithm, intending to increase the level of detail visible in an image, focuses on changing the luminescence L of a HDR image. The recorded gray value of a pixel (in an Analog-Digital-Unit (ADU)) is proportional to the luminance L (in the specific direction from which the pixel receives light)

$$L_{\text{Reinhard}} = \frac{L}{1+L} \tag{3}$$

These non-linear adjustments darken heavily overexposed areas of the image, while lower gray values remain nearly unchanged. This function is the most simple algorithm to achieve an image of increased perceptibility of objects for the human eye. The function is implemented as a class [15] in $OpenCV$ and is used for evaluation in this paper.

The Mantiuk [3] tone mapping operator uses the following equation

$$L_{\text{Mantiuk}} = \frac{L}{1+(L/\beta)^2} \tag{4}$$

The parameter β preserves fine details, by controlling the contrast retained in mid-tones, which makes it more suitable for images with a high level of textures. To calculate the images with Mantiuk's algorithm, the corresponding class [16] in $OpenCV$ was used.

The Drago [4] tone mapping operator is particularly known for its ability to handle very high dynamic ranges, without causing halo artifacts or excessive contrast reduction. It is based on the human visual system (HVS), emphasizing visibility and detail preservation, especially in shadowed areas. Therefore, the resulting luminance L_{Drago} is a logarithmic function of the recorded luminance L

$$L_{\text{Drago}} = \frac{\log(1+\alpha L)}{\log(1+L_{\max})} \tag{5}$$

The strength of the tone mapping can be adjusted by the compression factor α. To remain inside the displayable range, a normalization via the maximum luminance $L_{\max}$ of the image is implemented in this algorithm. Like the other tone mapping algorithms, a pre-defined class [17] in $OpenCV$ is also used for evaluation.

IV. RESULTS AND EVALUATION

The methods described in Section III are now applied. Overall 27 images of different scenes with changing light and ship positions were evaluated. The images are processed as 12-bit gray value images and downscaled to 8-bit images during tone mapping. However, to allow comparison of the individual processing steps in this paper, the images are also displayed as 8-bit images after each presented processing step.

To illustrate the steps of image post-processing, an example image was chosen. The scene (Fig. 2a) shows a ship at night, acquired with the VIS-NIR camera. The image has been acquired using the sensor system's active illumination at 808 nm and the first 50 m were gated-out to reduce atmospheric backscattering as explained above. The ship has a length of 28 m and was 983 m away. The image was taken at 18:37 UTC at 11.03.2024, which is about an hour after sunset on that day. The environment was dark and was only highlighted by navigational indication lights. The background and the water in the image is dark, which is an advantage of active illumination, as light is mostly reflected away from the instrument by specular reflection on the water surface. Only diffuse scattering and light, that is reflected by structures, that have a surface directed to the sensor system, is recorded. In comparison, the same scene recorded with the IR camera is plotted in Figure 2b.

In the IR image, the ship is clearly visible, but in contrast to the active illuminated image, the background (water) is visible

DOI: 10.5281/zenodo.17119990

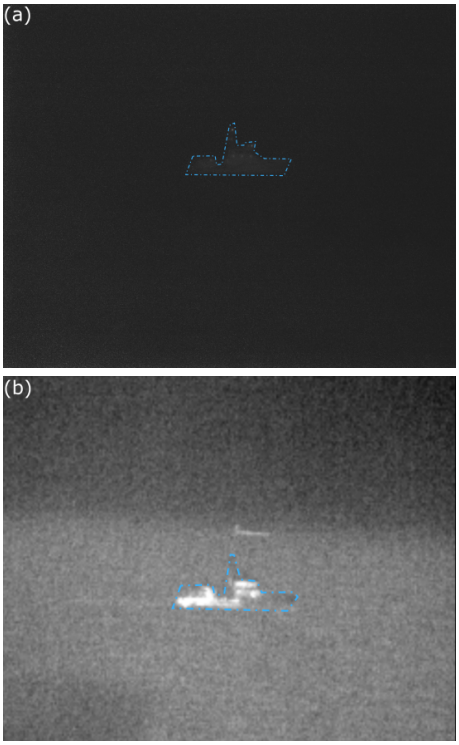

Fig. 2. (a) Image recorded with VIS-NIR camera and active illumination, (b) section of same scene recorded with thermal camera

as well. In addition, the thermal image contains more noise compared to the VIS-NIR channel acquired by a silica-based CMOS camera.

For better detectability of the ship in the image, only a section of 400 x 221 pixels is shown for the processed images. The cropped part of the image is black and does not differ from the background shown in the image.

The images in Figure 3 show the results after 1-point NUC as introduced in Section III-A, without and with added mean value of the image. The ship without the added mean value

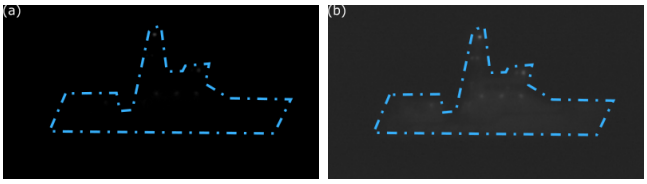

Fig. 3. (a) Image after 1-point NUC, (b) image after 1-point NUC plus average. These images demonstrate the human eyes problems to distinguish between dark gray levels.

(Eq. 1, Fig. 3a) is not or only hardly perceivable for the human eye. Adding the mean value to the image (Eq. 2, Fig. 3b) increases the visibility of the ship for the human eye.

The next filtering step is to reduce the stochastic noise (Sec. III-B), by applying Gaussian filtering (Fig. 4a) or performing a FFT (Fig. 4b). To recognize any difference and for the next tone mapping step, the image after 1-point NUC with added average value (Fig. 3b) was used.

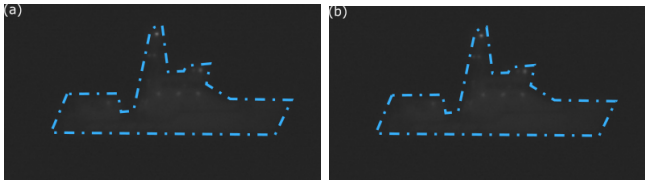

Fig. 4. (a) Image after 1-point NUC plus average and Gauss filtering (kernel size = 5 x 5, σ = 1), (b) Image after 1-point NUC plus average and FFT filtering (FFT mask: all elements equal 1, except center element, that is 0)

In the following, the most promising combinations of enhancement methods (NUC, temporal noise reduction, tone mapping) are discussed.

After reducing noise and evaluating the tone mapping algorithms from Subsection III-C, the best starting point for tone mapping is by using the 1-point NUC with added mean value and using one of the stochastic noise filters according to Fig. 4. The noise after Gaussian filtering (Fig. 4a) appears to be lower than after the FFT (Fig. 4b).

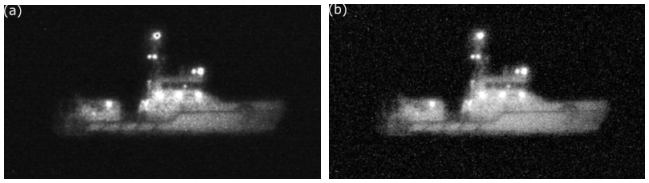

Fig. 5. (a) Image after 1-point NUC plus average, Gauss filtering and tone mapping according to Drago algorithm ($\alpha = 0.7$), (b) Image after 1-point NUC plus average, FFT filtering and tone mapping according to Drago algorithm ($\alpha = 0.7$)

In Figure 5 both random noise filters are presented, after tone mapping with the Drago algorithm. In Figure 5a the tone mapped image with Gaussian filtering (cf. Fig. 4a) and respectively in Figure 5b the result after tone mapping with FFT (cf. Figure 4b) are shown. In both images details, like windows, can be detected. The main difference is the intensity of both images. The ship is brighter with FFT filtering, but appears to be more noisy in the rest of the image.

In contrast, by applying the Reinhard and Mantiuk algorithms for the pre-filtered image, the quality of the resulting images with Gaussian filtering (cf. Fig. 4a) is decreased, so that the ship is more difficult to recognize (Fig. 6). The image

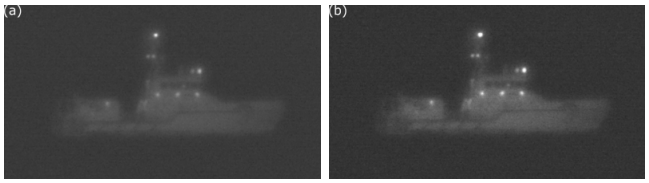

Fig. 6. (a) Image after 1-point NUC plus average, Gaussian filtering and tone mapping according to Reinhard algorithm, (b) image after 1-point NUC plus average, Gaussian filtering and tone mapping according to Mantiuk algorithm ($\beta = 0.3$)

after using the Reinhard operator (Fig. 6a) looks particularly blurred and it is difficult to recognize details. The Mantiuk operator also results in a slightly blurred effect, making it

DOI: 10.5281/zenodo.17119990

look as if a gray mask has been laid over the image (Fig. 6b). Although the beta parameter can still be adjusted with the Mantiuk operator, this leads to clipping in the area of the ship's position lights, which means that details in these areas are no longer recognizable.

FFT filtering (cf. Figure 4b) provides, as a basis, a higher perceptibly for both operators (Fig. 7). After using the Reinhard operator (Fig. 7a), it also appears as in Figure 6b, that a gray veil has been placed over the image. However, more details are visible in comparison. The resulting image after applying the Mantiuk operator (Fig. 7b) has a comparable intensity, than after FFT filtering with the Drago operator (Fig 5b), but details are still less perceptible.

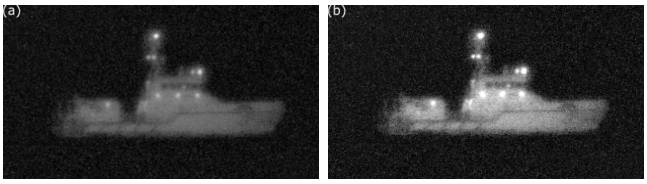

Fig. 7. (a) image after 1-point NUC plus average, FFT filtering and tone mapping according to Reinhard algorithm, (b) image after 1-point NUC plus average, FFT filtering and tone mapping according to Mantiuk algorithm ($\beta = 0.3$)

As proposed in Preis et al. [1], the SNR and C_M were used to quantify the results, additionally the CNR is introduced. Before the calculation of the SNR, C_M and CNR, the regions of interest (ROI) for calculation are defined like in Figure 8.

Fig. 8. ROIs for SNR and contrast calculation; red rectangle inside of ship hull (high intensity); blue rectangle outside of ship (low intensity)

The SNR is calculated for the ships hull (gray values in red rectangle x_{red}) and is computed as the mean value of the signal $\overline{\boldsymbol{x_{red}}}$ divided by the standard deviation $\sigma_{x_{red}}$ of the signal

$$SNR = \frac{\overline{\boldsymbol{x_{red}}}}{\sigma_{x_{red}}} \tag{6}$$

The contrasts are calculated as the ratio of gray values of the rectangle inside the ship (gray values in red rectangle x_{red} in Fig. 8) and the background (gray values in blue rectangle x_{blue}).

Therefore, the Michelson contrast is the sum of calculating the darker region of interest (gray values in blue rectangle x_{blue} in Fig. 8) with the region of interest inside the ships hull (gray values in red rectangle x_{red})

$$C_M = \frac{\overline{\boldsymbol{x}_{red}} - \overline{\boldsymbol{x}_{blue}}}{\overline{\boldsymbol{x}_{red}} + \overline{\boldsymbol{x}_{blue}}} \tag{7}$$

A value close to 0 indicates a low contrast, whereas a value close to 1 indicates a high contrast. It is a good measure, when the background is mainly dark and only objects of interest stand out. The disadvantage of this metric is its dependence on noise, as it is calculated using the mean values of the ROIs. This led to problems with the evaluation in Preis et al. [1]. For this reason, among others, the additional filtering of stochastic noise was introduced.

To obtain the contrast of the object in relation to the noise, the CNR is calculated. To do this, the mean value of the ships hull ($\boldsymbol{x}_{red}$) is subtracted by the mean value of the background ($\boldsymbol{x}_{blue}$) and divided by the root of the sums of the standard deviations σ of the red and blue rectangle

$$CNR = \frac{|\overline{\boldsymbol{x_{red}}} - \overline{\boldsymbol{x_{blue}}}|}{\sqrt{\sigma^2_{x_{red}} + \sigma^2_{x_{blue}}}} \tag{8}$$

The higher the value, the better the contrast, also in relation to the noise.

In Table I the resulting SNR, C_M and CNR for the image data set are summarized. In the first row, the results for the recorded images without image-processing are listed, in order to obtain a basis for the significance of the subsequent processing steps and their results in this table.

TABLE I
SIGNAL-TO-NOISE RATIOS, MICHELSON CONTRASTS AND CONTRAST-TO-NOISE RATIOS FOR OVERALL IMAGE DATA SET

Processed Image	∅ SNR	∅ C_M	∅ CNR
RAW image	9	0.07	1
NUC + mean, Gauss, Reinhard	11	0.23	2
NUC + mean,Gauss, Mantiuk	11	0.30	2
NUC + mean,Gauss, Drago	9	0.36	1
NUC + mean,FFT, Reinhard	4	0.41	2
NUC + mean,FFT, Mantiuk	6	0.37	2
NUC + mean,FFT, Drago	3	0.50	3

As stated in Subsection III-C, tone mapping operators also increase noise. For this reason, the SNR has hardly changed and has even become worse in certain algorithm combinations. However, the contrast has been increased. The C_M and CNR are consistent in their findings on contrast, even if the gradations with the C_M are finer with the CNR.

The algorithm combination of "NUC + mean, Gauss, Drago" stands out here, as it provides a comparable contrast improvement to the FFT. With the FFT, the Drago operator has the highest Michelson contrast with a $C_M = 0.50$. The CNR with this operator is also the highest for the data set, whereas the SNR is the lowest. This is due to the calculation of the gray values, which are a logarithmic function of the raw values (Eq. 5). As a result, the noise for certain gray value ranges is increased more than with the other two operators.

In principle, the CNR has been increased and is also consistent with the results with the C_M. The assertion from Preis et al. [1], that the C_M is only limited useful in the evaluation of monochrome images is conditionally true, as the noise was further reduced by the additional filter step and therefore, the informative value of the C_M for this type of images became the same as the CNR.

DOI: 10.5281/zenodo.17119990

V. CONCLUSION

Measurements were performed during nighttime at sea using a multi-sensor instrument (Sec.II). The IR camera gives a good overview over a scene with a larger field of view. For a more detailed inspection or an unclear detection on the IR image (that has usually a limited resolution), the VIS-NIR camera is preferred.

In the first image processing step, camera-characteristic systematic differences in the dark signal, i.e. the dark signal non-uniformity was corrected by a 1-point NUC (Sec. III-A). In theory, the different pixel-sensitivity, i.e. the photo-response non-uniformity, could be corrected as well using a 2-point NUC. However, most of the images above water are dark as a result of active illumination reflected away from the instrument by the water surface. On the other hand, metallic surfaces and retro reflections from other ships dominated, whenever other ships were inside the field of view. This leads to saturated pixels, that are not corrected by a 2-point NUC.

In the second step (Sec. III-B), the stochastic noise was reduced using either the Gaussian filter or a FFT mask. The Gaussian filter reduces the noise better than the FFT would do. However, the FFT with the tone mapping operators provides better results in terms of increasing the contrast.

In the final step, the visibility of objects at sea and at night was then assessed by adjusting the contrast by the three tone mapping operators (Sec. III-C). The Drago operator stands out here, as it increases the contrast the most. However, it also increases the noise the most. The Reinhard and Mantiuk operators also deliver good results for increasing the contrast.

The image post-processing techniques presented here are well-known and form the basis for further investigations in image-enhancing for monochrome images at night and sea. Especially in the area of tone mapping operators, there are many others [5], that can be investigated for this special scenario. The improvement of IR images should also be investigated independently of VIS images like in Dulski et al. [18].

To summarize, the noise reduction methods presented and the subsequent contrast enhancement using one of the tone mapping operators, can increase the detectability of objects at sea at night (Sec. IV). It was also shown, that an increased contrast is accompanied by increased noise. However, as the majority of such images is black and only objects floating on the water reflect light, high contrast is more important than reduced noise. This means, that there is also a chance, a human operator will be able to detect weakly reflective objects.

Building on this study, evaluations can now be carried out with test subjects, who represent the human operator during a search and rescue operation, so that the results obtained here, can also be assessed quantitatively. A further study can also investigate, how an automated object detector can support the human operator. The probability of detection and also the speed of detection with and without an object detector should be evaluated. The pre-trained object detector YOLOv8 from Preis et al. [1] could be a starting point.

ACKNOWLEDGMENT

We thank the Federal Maritime and Hydrographic Agency (Bundesamt für Seeschifffahrt und Hydrographie, BSH), its employees and especially the crew of the Survey, wreck-search and research vessel ATAIR for the chance to participate in the field trip for collecting the underlying data set of this study.

REFERENCES

[1] T. Preis, J. Schmidt, A. Klein, E. Peters, T. Lübcke, and M. Stephan, "Optimizing postprocessing of range-gated viewing data for maritime search and rescue operations at night and in bad weather conditions," *Transactions on Maritime Science*, vol. 13, no. 1, 2024.

[2] E. Reinhard, M. Stark, P. Shirley, and J. Ferwerda, "Photographic tone reproduction for digital images," *ACM Transactions on Graphics*, vol. 21, no. 3, pp. 267–276, 2002.

[3] R. Mantiuk, S. Daly, and L. Kerofsky, "Display adaptive tone mapping," in *ACM SIGGRAPH 2008 papers*, ser. ACM Conferences. New York, NY: ACM, 2008, pp. 1–10.

[4] F. Drago, K. Myszkowski, T. Annen, and N. Chiba, "Adaptive logarithmic mapping for displaying high contrast scenes," *Computer Graphics Forum*, vol. 22, no. 3, pp. 419–426, 2003.

[5] S. Yelmanov and Y. Romanyshyn, "Automatic enhancement of low-contrast monochrome images," in *2018 IEEE 38th International Conference on Electronics and Nanotechnology (ELNANO)*. Piscataway, NJ: IEEE, 2018, pp. 587–593.

[6] A. A. Michelson, *Studies in Optics*. The University of Chicago Press, 1927.

[7] E. Peters, J. Schmidt, Z. Jurányi, M. W. Berger, S. Scherbarth, and F. Lehmann, "Development of a novel low-cost nir gated-viewing sensor for maritime search and rescue applications," in *Electro-Optical Remote Sensing XIII*, ser. Proceedings of SPIE, G. W. Kamerman and O. Steinvall, Eds. Bellingham, Washington, USA: SPIE, 2019, p. 3. [Online]. Available: https://www.spiedigitallibrary.org/conference-proceedings-of-spie/11160/2532538/Development-of-a-novel-low-cost-NIR-gated-viewing-sensor/10.1117/12.2532538.full

[8] D. L. Perry and E. L. Dereniak, "Linear theory of nonuniformity correction in infrared staring sensors," *Optical Engineering*, vol. 32, no. 8, p. 1854, 1993.

[9] T. Kimpe and T. Tuytschaever, "Increasing the number of gray shades in medical display systems–how much is enough?" *Journal of digital imaging*, vol. 20, no. 4, pp. 422–432, 2007.

[10] A. Makandar and B. Halalli, "Image enhancement techniques using highpass and lowpass filters," *International Journal of Computer Applications*, vol. 109, no. 14, pp. 21–27, 2015.

[11] R. A. Haddad and A. N. Akansu, "A class of fast gaussian binomial filters for speech and image processing," *IEEE Transactions on Signal Processing*, vol. 39, no. 3, pp. 723–727, 1991.

[12] OpenCV, "Home," 10.02.2025. [Online]. Available: https://opencv.org/

[13] "Opencv: Smoothing images," 12.02.2025. [Online]. Available: https://docs.opencv.org/4.x/d4/d13/tutorial_py_filtering.html

[14] "Legacy discrete fourier transforms (scipy.fftpack) — scipy v1.15.1 manual," 11.01.2025. [Online]. Available: https://docs.scipy.org/doc/scipy/reference/fftpack.html

[15] "Opencv: cv::tonemapreinhard class reference," 13.02.2025. [Online]. Available: https://docs.opencv.org/4.x/d0/dec/classcv_1_1TonemapReinhard.html

[16] "Opencv: cv::tonemapmantiuk class reference," 13.02.2025. [Online]. Available: https://docs.opencv.org/4.x/de/d76/classcv_1_1TonemapMantiuk.html

[17] "Opencv: cv::tonemapdrago class reference," 13.02.2025. [Online]. Available: https://docs.opencv.org/4.x/da/d53/classcv_1_1TonemapDrago.html

[18] R. Dulski, P. Powalisz, M. Kastek, and P. Trzaskawka, "Enhancing image quality produced by ir cameras," in *Electro-Optical and Infrared Systems: Technology and Applications VII*, ser. SPIE Proceedings, D. A. Huckridge and R. R. Ebert, Eds. SPIE, 2010, p. 783415.

DOI: 10.5281/zenodo.17119990